



HAL
open science

A new robust modeling strategy for multi-component droplet heat and mass transfer in general ambient conditions

Fernando Luiz Sacomano Filho, Artur Carvalho Santos, Aymeric Vié, Carlos Krieger Guenther

► **To cite this version:**

Fernando Luiz Sacomano Filho, Artur Carvalho Santos, Aymeric Vié, Carlos Krieger Guenther. A new robust modeling strategy for multi-component droplet heat and mass transfer in general ambient conditions. *International Journal of Heat and Mass Transfer*, 2022, 194, pp.123102. 10.1016/j.ijheatmasstransfer.2022.123102 . hal-03513783v2

HAL Id: hal-03513783

<https://hal.science/hal-03513783v2>

Submitted on 16 Jan 2023

HAL is a multi-disciplinary open access archive for the deposit and dissemination of scientific research documents, whether they are published or not. The documents may come from teaching and research institutions in France or abroad, or from public or private research centers.

L'archive ouverte pluridisciplinaire **HAL**, est destinée au dépôt et à la diffusion de documents scientifiques de niveau recherche, publiés ou non, émanant des établissements d'enseignement et de recherche français ou étrangers, des laboratoires publics ou privés.

A new robust modeling strategy for multi-component droplet heat and mass transfer in general ambient conditions

Fernando Luiz Sacomano Filho^{a,*}, Artur Carvalho Santos^b, Aymeric Vié^{b,c}, Guenther Carlos Krieger Filho^a

^a*Laboratory of Environmental and Thermal Engineering, Universidade de São Paulo, São Paulo, Brazil.*

^b*Laboratoire EM2C, CNRS, CentraleSupélec, Université Paris-Saclay, Gif-sur-Yvette, France.*

^c*Fédération de Mathématiques, CentraleSupélec, Université Paris-Saclay, Gif-sur-Yvette, France.*

Abstract

Liquid fuels used for spray combustion processes are predominantly composed of several mixed components. The atomization of a liquid jet forms multi-component liquid droplets. These droplets are subject to heat and mass transfers in a vast range of atmosphere configurations, resulting in complex interactions. This example of spray combustion summarizes the diversity of scenarios that a droplet may experience in a spray flow. Unfortunately, available models in the literature exhibit limitations for characterizing such complex interactions. This work proposes a novel modeling strategy to account for such interactions in diverse scenarios grounded in a consistent computational approach. We derive a new formulation from general transport equations of the gas phase. We validate the resulting model by comparing numerical results with available experimental data and consider binary mixtures of liquids evaporating in different ambient conditions. Compared to other reference approaches, the proposed model proves to be efficient in all tested scenarios, including severe atmosphere compositions and states. Additional differential diffusion effects among participating species are observed, not only for mass but also for heat transfer.

Keywords: Droplet evaporation, Evaporation modeling, Multi-component droplets, Spray combustion, Differential diffusion, Ethanol

*Corresponding author

Email address: fernando.sacomano@usp.br (Fernando Luiz Sacomano Filho)

1. Introduction

When considering combustion processes of hydrophilic fuels, a challenging scenario emerges: droplet heat and mass transfer processes in atmospheres with high mass fractions of a liquid vapor species. Concretely, these conditions can be present, for example, during the interaction of hydrox ethanol droplets with combustion products, where high mass fractions of water vapor exist. Such a scenario imposes constraints concerning evaporation and condensation during the droplet lifetime [1], which is a quite challenging task for heat and mass transfer modeling. This is not limited to liquid hydrophilic fuels, as it may occur in any flow where liquid droplets interact with atmospheres composed of varying vapor mass fractions crossing their corresponding saturation values.

To handle phase change in such conditions, one of the most important physical phenomena is the vapor diffusion into the surrounding gas. For single-component droplets, many models have been derived and are canonically used for combustion applications [2–4]. For multi-component vaporization, fewer contributions can be found [1, 5–9] and no model emerge as a reference. However, as already pointed out by Brenn et al. [5], there is a need for a realistic description of the heat and mass transfers across the interface between phases, in order to achieve a thorough description of multi-component droplet evaporation. Therefore, the derivation of reliable and computationally efficient models able to accurately represent the differential diffusion transport among species and energy is desired.

Focusing on recent related works, Tonini and Cossali [7] presented a comparative analysis between different approaches, which may account for the differential diffusion effects of evaporating liquid droplets. Two models have been proposed: an analytical model that accounts for the inter-species mass diffusion in the gaseous mixture and another model based on a single-component analogy. Additionally, a novel solution strategy is proposed for the model based on the detailed description of diffusion transport, which contrasts with the one presented in [10]. In both [7] and [10], Fick’s law is applied for diffusion, while heat transfer follows the formulation of Abramzon and Sirignano [11]. The differential diffusion is considered in [5] under the assumption that each species interacts singly as a binary mixture with the surrounding air, following the ideal

gas approach. Results show a good agreement with experimental data obtained from acoustically-levitated droplets. Recently, this model was applied in [9] to study the evaporation of ethanol/water droplets at different ambient conditions, including variations in relative air humidity. Fang et al. [8] also analyzed single droplet evaporation of different liquid mixtures with a modeling approach based on the one proposed in [5] but including radiation effects.

Ebrahimian and Habchi [6] present a multi-component approach based on the so-called Hirschfelder-Curtiss approximation (e.g. [12, 13]). The resulting method is based on an iterative procedure to solve the mass flow rate, droplet temperature, and composition of the liquid and gas mixtures. Their results showcase a good representation of trends observed experimentally for binary mixtures of n-heptane and n-decane. Focusing on binary mixtures of ethanol and water, Lupo and Duwig [14] performed numerical investigations of different initial droplet compositions and effects of preferential diffusion of liquid vapor into the surrounding gas. To account for preferential diffusion, an approach is proposed to address the enthalpy fluxes caused by the different species-specific heats into the gas energy equation. Despite the special attention given to ethanol and water binary mixtures, the validation of the resulting multi-component model is limited to n-heptane and n-decane mixtures.

All listed models fail to capture the transition between evaporation and condensation during the droplet lifetime, at least in their original form, which is mandatory to describe the vaporization of multi-component droplets composed of hydrophilic species. To fulfill this objective, the present work proposes a novel approach for the modeling of multi-component droplet heat and mass transfer, which is rigorously derived from general transport equations of the gas phase. Specific attention is devoted to the determination of vapor-liquid equilibrium [15] and diffusion coefficients. Although the proposed model has no limitation to the number of liquid compounds, the presented investigations focus on binary mixtures of various substances. Still, it is important to point out that the resulting model would not easily reach its full functionality with typical solution procedures applied to droplet heat and mass transfer simulation. To that end, a novel solution strategy is developed and applied throughout this work.

The remainder of this manuscript is divided into seven sections. The modeling techniques are first presented concisely, whereas specific model derivations are placed in the supplementary

material. Then, the solution strategy is presented, which is of fundamental importance to solve the resulting equations with the proposed modeling approach. Results are distributed in four sections, where different topics are systematically investigated. Finally, the paper is closed with some final remarks and outlooks.

2. Modeling description

In this section, our new modeling approach is described. Initially, a description of how the heat and mass transfers are handled in the gas and liquid phases is presented. The adaptation to convective effects is also included. The computation of the diffusion coefficients and the vapor-liquid equilibrium (VLE) is finally presented.

2.1. Heat and mass transfer on a quiescent atmosphere: gas phase

The key aspects of the model derivation process are summarized in this section in Eqs. 1-6 for the energy, mass, and species conservation. These formulations have been derived from the transport equations of energy and chemical species of the gas phase as detailed in the supplementary material, wherein modeling assumptions are gradually presented as soon as they are employed. Altogether, these can be summarized as:

1. Ambient conditions of droplet surroundings taken to be uniform, e.g. droplet-droplet interactions are not accounted for;
2. Quasi-steady process;
3. Spherical symmetry;
4. Heat conduction is expressed in terms of Fourier's law;
5. Mass diffusion is expressed in terms of Fick's law;
6. Second order Soret and Dufour effects are neglected for heat and mass diffusion;
7. Source terms related to the species consumption (or production), as well as heat release due to chemical reactions, are neglected;
8. The low-Mach dilatable hypothesis is enforced;
9. Volumetric forces are not taken into account;

10. No net dissolution of inert gases onto the liquid phase;
11. Ideal gas formalism employed for the gas phase¹;
12. Constant thermodynamic and transport properties in the gas phase. These properties are computed using the one-third rule for mass fractions and temperatures [16]. The dynamic viscosity and thermal conductivity are averaged using Wilke's rule as in [2].

The energy conservation, here presented through the sensible enthalpy h , takes the following form after some manipulations:

$$\frac{d}{dr}(\rho u r^2 h) - \frac{d}{dr}\left(\lambda r^2 \frac{dT}{dr}\right) - \frac{d}{dr}\left(\sum_{k=1}^N \rho D_k h_k r^2 \frac{dY_k}{dr}\right) = 0, \quad (1)$$

where ρ is the density, u is the velocity, r is the radial coordinate, λ is the thermal conductivity, T is the temperature, D_k are the diffusion coefficients from species k towards the multi-component gas mixture, and Y_k is the mass fraction. After integration, the following form is retrieved:

$$\begin{aligned} \dot{m} c_p [T(R) - T_s] - 4\pi \lambda R^2 \frac{dT}{dR} - 4\pi \sum_{k=1}^N h_k \left(\rho D_k R^2 \frac{dY_k}{dR} \right) = \\ - \underbrace{4\pi R_d^2 \lambda \frac{dT}{dR} \Big|_{R_d}}_{\dot{q}_d} - 4\pi \left[\sum_{k=1}^N h_{k,s} \left(\rho D_k R_d^2 \frac{dY_k}{dR} \Big|_{R_d} \right) \right], \end{aligned} \quad (2)$$

where \dot{q}_d is the heat transfer rate necessary to raise droplet temperature and c_p is the specific heat at constant pressure. Subscript s refers to quantities evaluated at the droplet surface. A second integration allows the isolation of the aforementioned heat transfer rate; however, both terms in parentheses make this a challenging task. One of the main contributions of the proposed model is the approach chosen to address this issue. For that, it is necessary to proceed with the transport equation for each species k :

$$\frac{\dot{m}}{4\pi} \frac{dY_k}{dr} - \frac{d}{dr} \left(\rho D_k r^2 \frac{dY_k}{dr} \right) = 0, \quad (3)$$

¹Even though the ideal gas simplification is assumed, non-ideal effects are considered in the liquid phase and the phase interface.

which when integrated and combined with the definition of the fractional evaporation rate of species k ($\varepsilon_k = \dot{m}_k/\dot{m}$) presented in [17] concerning the Fick's Law assumption, leads to the following expression:

$$\dot{m}[Y_k - \varepsilon_k] - 4\pi\left(\rho D_k R^2 \frac{dY_k}{dR}\right) = 0. \quad (4)$$

Note that considering all participating vapor species k , it follows that $\sum_k \varepsilon_k = 1$, or accordingly $\sum_k \dot{m}_k = \dot{m}$. Through integration, the global evaporation rate can be expressed as function of any species k :

$$\dot{m} = -\dot{m}_d = 4\pi R_d \rho D_k \ln |B_{M,k} + 1|, \quad (5)$$

where R_d is the instantaneous droplet radius. The presence of the absolute value in this expression is of great importance, as it is the first ingredient required to handle condensation and vaporisation switching during the droplet lifetime, which is a novelty of this work.

A key aspect of the derivation process is highlighted in Eq. 4, namely the term in parentheses being the same as the first term in parentheses in Eq. 2. Therefore, Eq. 2 is rearranged and combined with 4. Similarly, the second term in parentheses in Eq. 2 can be substituted by the definition of ε_k , as done from Eq. 3 to Eq. 4. As a result, the energy equation can be integrated and the heat transfer rate isolated as follows:

$$\dot{q}_d = \dot{m}_d \left[L - \frac{\sum_k c_{p,k} \varepsilon_k (T_\infty - T_s)}{B_T} \right], \quad \text{with} \quad L = \sum_k L_k \varepsilon_k, \quad (6)$$

in which L is the latent heat of the mixture and L_k the latent heat of species k . Subscript ∞ refers to quantities evaluated in the far field. In contrast to other modeling approaches, not only the latent heat but also the sensible heat flux is expressed in terms of the fractional evaporation rate ε_k . This is a straight outcome of the previously described coupling procedure between energy and species transport equations. As such, evaporation and condensation mechanisms can be comprehensively taken into account for both latent and sensible heat fluxes. Further, subscripts d and l are associated with droplet and liquid quantities. For more details about the derivation procedure, the reader is referred to the supplementary material.

The terms B_T in Eq. 6 and $B_{M,k}$ in 5 refer to the Spalding transfer numbers for energy and

species k . Both are described by:

$$B_T = \frac{(T_\infty - T_s) \sum_k c_{p,k} \varepsilon_k}{L - \frac{\dot{q}_d}{\dot{m}_d}}, \quad \text{and} \quad B_{M,k} = \frac{Y_{k,s} - Y_{k,\infty}}{\varepsilon_k - Y_{k,s}}. \quad (7)$$

From the derived set of equations, it is important to note that, in typical situations² when the diffusion coefficient D_k and the Spalding mass transfer number $B_{M,k}$ are determined, the droplet global net flux \dot{m}_d is obtained in terms of Eq. 5. Such an observation may lead to the interpretation that the contribution of only a single species is necessary for this computation. Nevertheless, this is not consistent, as information about all other participating species are implicitly included in ε_k , since the condition $\sum_k \varepsilon_k = 1$ must be attained.

If the simplification that all participating species present the same value for the diffusion coefficient is made, the determination of ε_k is straightforward. Under this condition, Eq. 5 would lead to $B_{M,k} = B_M$ for all k (see for instance [3]). However, the inclusion of differential diffusion effects leads to additional computational efforts in order to compute the ε_k .

The presence of the absolute operator in some expressions turns the solution of the derived equations into a challenging task. An adapted and consistent solution procedure is proposed in section 3.

2.2. Heat and mass transfer on a quiescent atmosphere: liquid phase

The equations presented in the previous section, which determine heat and mass transfer rates, have been derived considering only the gas phase. The resulting set of equations may lead to the interpretation that liquid phase information is not necessary; however, such information is hidden in quantities evaluated at the droplet surface. Before addressing the approaches employed to describe the phase interface, the treatment given for the liquid phase is indicated.

The so-called infinite liquid conductivity and diffusivity (ILCD) approach is used to describe the liquid phase. Influences of the spatial resolution of the droplet interior on the proposed model will be the subject of subsequent works. A zero-dimensional approach is obtained following the assumptions of spherical symmetry, quiescent atmosphere, and absence of gravity effects.

²Exceptions occur when the argument of the logarithm operator in Eq. 5 presents a singularity (e.g. $Y_{k,s} = Y_{k,\infty}$)

In agreement with the ILCD approach, the temperature within a droplet is uniform, even though it may vary along with time. An expression for it can be determined considering the heat transfer rate necessary to raise droplet temperature \dot{q}_d , as follows

$$mc_l \frac{dT_d}{dt} = \dot{q}_d \Rightarrow \frac{dT_d}{dt} = \frac{\dot{q}_d}{mc_l}, \quad (8)$$

where t is time, m the droplet mass at t , and c_l the liquid specific heat.

Concerning the mixture composition in the liquid phase, the hypothesis of infinite liquid diffusivity leads to uniform values of species molar fractions within a droplet. As for the liquid temperature under the ILCD approach, the mixture composition may vary over time. However, its determination is straightly achieved when solving the entire equation set, which includes the phase interface modeling.

2.3. Convective heat and mass transfer

Care must be taken to consider convective heat and mass transfer on a multi-component droplet while preserving the generality of the proposed approach. As a result of the derivations presented in the supplementary materials, convective heat and mass transfers can be considered in terms of

$$\dot{q}_d = 4\pi R\lambda \frac{Nu}{2} (T^\infty - T^s) - \dot{m}L \quad \text{and} \quad \dot{m} = 4\pi R\rho D_k \frac{Sh_k}{2} B_{M,k}. \quad (9)$$

Both equations are general and can therefore be applied to describe evaporation and condensation processes. However, limitations may arise according to the strategy adopted to compute the Nusselt Nu and the Sherwood Sh_k numbers.

In agreement with the classical model [15], a general approach is to consider that

$$Nu = \frac{\ln |B_T + 1|}{B_T} Nu^0 \quad \text{and} \quad Sh_k = \frac{\ln |B_{M,k} + 1|}{B_{M,k}} Sh_k^0, \quad (10)$$

where Nu^0 refers to empirical correlations derived from non-evaporating moving droplets, and Sh_k^0 is the analogous for mass transfer with Pr replaced by Sc (see Eq. 11). For instance, in the present work we employed the following expressions

$$Nu^0 = 2 + 0.57Re^{1/2}Pr^{1/3} \quad \text{and} \quad Sh_k^0 = 2 + 0.57Re^{1/2}Sc_k^{1/3}, \quad (11)$$

where $Re = \rho|u_\infty - u_d|d_p/\mu$ is the Reynolds number, u_∞ the velocity of the bulk flow, u_d the droplet's velocity, d_p the droplet diameter, μ the dynamic viscosity, Pr the Prandtl number, and $Sc_k = \mu/\rho D_k$ the species k Schmidt number.

Specific limitations emerge when empirical correlations derived for evaporating droplets replace Nu and Sc_k in Eq. 9, or when models based on the film theory (e.g. [11]) are envisaged. When using these strategies, attention must be paid to the fact that equations have been derived for limited values for Spalding numbers. For example, in the Abramzon and Sirignano [11] model the Falkner-Skan solutions (see [3]) used to obtain the correction factor F were derived for a range of $0 \leq B \leq 20$ [15], where B refers either to B_T or B_M . Specifically to the Abramzon and Sirignano [11] model, a strategy to attenuate such limitations is to consider a Spalding number based on the gaseous mixture for the computation of F as proposed by Tonini and Cossali [7]

$$B_M = \frac{\sum_{\text{vapor}} Y_k^s - \sum_{\text{vapor}} Y_k^\infty}{1 - \sum_{\text{vapor}} Y_k^s}, \quad (12)$$

where the subscript vapor implies the summation is ignoring all inert species. Accordingly, the limitations presented by possible negative values of $B_{M,k}$ are attenuated by the summation operator. Nevertheless, this approach implies that differential diffusion effects are neglected³ within the film, even though this is considered when computing the modified Nusselt and Sherwood numbers as follows

$$Nu^* = 2 + \frac{Nu^0 - 2}{F_T} \quad \text{and} \quad Sh_k^* = 2 + \frac{Sh_k^0 - 2}{F_M}, \quad (13)$$

in which F_T and F_M are the correction factors respectively for thermal and species k film thicknesses due to Stefan flow effects, given by

$$F = (1 + B)^{0.7} \frac{\ln(B + 1)}{B}, \quad (14)$$

where B refers to B_T and B_M correspondingly.

2.4. Modeling of diffusion coefficients

As the evaporation rates are proportional to mass diffusion coefficients a particular attention must be devoted to their evaluation, specifically on two aspects: the determination of binary dif-

³The Spalding number of the gas mixture is obtained when the assumption that all participating species have the same value for the diffusion coefficient (i.e. $D_k = D$) is made.

fusion coefficients and the approaches used to estimate the diffusion coefficient of a species into a mixture. The last method is typically connected to the first one, as it is often formulated in terms of binary diffusion coefficients. Nevertheless, both approaches are independent and, for each one, different modeling strategies can be applied.

With respect to the approaches used to estimate binary diffusion coefficients, special attention is given to the so-called Fuller method (FM) [18–20] due to its use in previous works (e.g. [4, 21]) and its additive formulation which aligns with the UNIFAC approach (see section 2.5). According to this method, binary diffusion coefficients can be estimated by

$$D_{ij} = 0.00143 \frac{T^{1.75} \left(\frac{1}{M_i} + \frac{1}{M_j} \right)^{1/2}}{P \sqrt{2} \left(\sum_i v_k^{1/3} + \sum_j v_k^{1/3} \right)^2}, \quad (15)$$

where M_i is the molar mass of species i , P the ambient pressure, and $\sum_i v_k$ the summation of atomic diffusion volumes that composes species i . The determination of the diffusion volumes is based on the application of a non-linear least squares optimization analysis over experimental databases of binary diffusion coefficients of various substances [18, 19]. In [18, 19], Fuller and co authors defined specific values of diffusion volumes for some molecules, which do not always coincide with the corresponding summation procedure of atomic diffusion volumes. In a first moment, this called our attention on how to represent the binary diffusion coefficient of ethanol with other substances, since our first investigations were conducted with ethanol/water mixtures and deviations were noticed between computations and experimental data. As noticed in Fig. A.2 (a), comparisons between experimental data and D_{ij} values obtained in the two cases labeled by *Air 1966* and *Air 1969* (both referring to computations performed with atomic diffusion volumes extracted respectively from [18] and [19]) show a better agreement with the lowest range of values achieved experimentally. Such a performance is also noticed for water diffusion in air, as presented in Fig. A.2 (b). Specific diffusion volumes are presented for water in [18, 19], which do not coincide with the corresponding summation of hydrogen and oxygen atomic volumes. The good agreement observed for water-air mixtures corroborates the observation made in [18] that the consideration of specific diffusion volumes for some substances improved model accuracy. Particularly, the experimental database employed in that work considered four data points for water-air mixtures

while only one for ethanol-air ($D_{ij} = 0.135 \text{ cm}^2/\text{s}$ at $T=298.2 \text{ K}$), which may point out that the consideration of additional experimental data could improve the predictive ability of the method for ethanol-air mixtures.

Rigorously, the diffusion of a substance in air is not a strict binary diffusion process since air is a mixture of predominantly two substances, i.e. oxygen O_2 and nitrogen N_2 . The constant composition of air in most engineering applications may be a justification to treat it as a pure substance, as done in [18] and [19]. Accordingly, diffusion volumes for air can be found. Thus, we investigate the behavior of the Fuller method when the diffusion of a substance in air is accounted for as a multi-component diffusion problem. Hence, in both Fig. A.2, results achieved following a multi-component diffusion modeling with diffusion volumes obtained in [18] and [19] are respectively presented under *MC 1966* and *MC 1969* labels. For such computations, it is assumed that the concentration of the vapor species does not interfere with the value of the multi-component and the binary diffusion coefficients as given by Eq. 17. The diffusion coefficients computed with the multi-component approach demonstrate a similar behavior when compared with the simplification of air as a single species in Fig. A.2. As for ethanol or water, the multi-component approach outputs greater values of diffusion coefficients in both scenarios, showing a better agreement with the experimental data. Hence, the Fuller method shows a better performance for the computation of diffusion coefficients of vapor in air when air is represented by a multi-component mixture.

As mentioned in [22], there is no consensus in the literature concerning the computation of multi-component diffusion coefficients D_k when Fick's Law is applied. Rigorously, the usage of multi-component diffusion coefficients D_k with Fick's Law requires an additional artifice to preserve both identities $\sum_{k=1}^N Y_k V_k = 0$ and $\sum_{k=1}^N Y_k = 1$ (V_k is the diffusion velocity - more details in the supplementary material). As pointed out in [17, 22], this artifice can be the consideration of a correction velocity or the specification of D_k for $N - 1$ species which are present in trace amounts. In our implementations, D_k is only computed for vapor species and no correction velocity is included. This approach does not differ from the applied strategies for instance in [7, 10] and resembles the second listed artifice to attain the two identities. Nevertheless, the impact of such an approach requires further studies which may be subject of future works.

Due to the previously mentioned lack of consensus concerning the computation of D_k , two

approaches have been analyzed in the present work. The first corresponds to the so-called Blanc's law [23, 24] which is commonly used in simulations of multi-component droplet evaporation [7, 21]. Following the formulation presented in [24, 25], D_k is given by

$$D_k = \left(\sum_{j \neq k}^N \frac{X_j}{D'_{kj}} \right)^{-1}, \quad (16)$$

where D'_{kj} refers to the binary diffusion coefficient of species k and j evaluated in the actual multi-component mixture. As mentioned in [25], D'_{kj} is not quite the same as the corresponding binary diffusion coefficient D_{kj} , where the difference between both corresponds to the weak dependence of D'_{kj} on the whole multi-component mixture composition. However, as already highlighted by Marrero and Mason [25], deviations between both coefficients are at most of few percent and the assumption $D'_{kj} \approx D_{kj}$ is a reasonable approach. Therefore, we assume that $D'_{kj} = D_{kj}$ in the present study. It is important to mention that some works present Eq. 16 in terms of mass fractions [7, 21], where X_j is switched by Y_j while $D'_{kj} = D_{kj}$.⁴

The second tested approach is given by

$$D_k = (1 - X_k) \left(\sum_{j \neq k}^N \frac{X_j}{D_{kj}} \right)^{-1}, \quad (17)$$

which is evaluated in [26] within the context of flame speed computations and pointed out in [17] as a quantitatively correct approach. By comparing Eq. 17 with Blanc's law, it is not difficult to identify that the term $(1 - X_k)$ in Eq. 17 turns D_k independent on the concentration of species k . Even though the studies presented by Sandler and Mason [24] and Marrero and Mason [25] indicated from derivations within the Chapman-Enskog kinetic theory that there is a dependence of the concentration of species k on D_k , experimental investigations presented in [27] demonstrated that such a dependence is not general. Studies conducted with diffusion of methanol and chloroform vapors at different molar fractions in air indicated that the multi-component diffusion coefficient varies for chloroform but is predominantly constant for methanol. Mrazek et al. [27] point out that the observed differences of substance behavior are assigned to the differences of substances'

⁴In all the computations performed here with models obtained from [7], calculations of D_k follows Eq. 16 expressed in terms of mass fractions.

mass fractions, which indicates an agreement with the rationale presented in the investigations performed for binary diffusion coefficients in [28] and [29]. Hence, for mixtures where participating species present similar molar masses, Eq. 17 may be a suitable approach.

In order to choose the right formulation for estimating the multi-component diffusion coefficient, we considered the following rationale. In [24], deviations from the Blanc's law were investigated by means of the Chapman-Enskog kinetic theory. There, the Chapman-Enskog method is algebraically manipulated to resemble Blanc's law. By comparing the resulting equation with that of Blanc's law, an expression for the deviation could be obtained. Sandler and Mason [24] presented solutions of the derived deviation equations only for the special case of diffusion of a trace species through a quiescent mixture, specifically when $X_k = 0.0$. Within this context, even though Blanc's law was demonstrated to be exact in certain cases, deviations due to variations on species mass fractions were not quantified. In view of this aspect, the low variation of diffusion coefficients with vapor molar fractions in experiments conducted in [27], and the high complexity associated with implementations of more accurate models, we preferentially use Eq. 17 in our implementations. Still, it should be noted that any alternative formulation for computing the diffusion coefficients of one species towards a mixture could be applied to the current modeling strategy with no further difficulties. A more detailed analysis of such approaches in multi-component droplet evaporation will be subject to future works.

2.5. Phase Interface: vapor liquid equilibrium

The description of the composition at the interface is of key importance to the entire modeling strategy. In the present study, it is assumed that thermodynamic equilibrium is maintained in all tested scenarios. Two approaches have been adopted to represent the so-called vapor-liquid-equilibrium (VLE).

Within the thermodynamic equilibrium hypothesis, the fugacity of a liquid species k equals the fugacity of its vapor. By considering the representation of the fugacity in terms of activity coefficients, the VLE hypothesis allows the expression of the molar fraction of liquid species k (X_k^L) in terms of the molar fraction of its vapor (X_k^V) as follows

$$X_k^V P = X_k^L \gamma_k P_{vp,k} \mathcal{F}_k, \quad (18)$$

where γ_k is the activity coefficient of species k , P_{vp} the vapor pressure, and \mathcal{F} a correction factor to include effects of real substances. Poling et al. [30] reference that for subcritical components, \mathcal{F}_k is often 1. Since our analyses are conducted at atmospheric pressure, this simplification is applied. Further simplifications can be done when γ_k is assumed as 1, which characterizes Raoult's law.

The two approaches applied to address the VLE refer to Raoult's law and the general UNIFAC activity coefficient model as described in [30]. This strategy, also adopted in different works (e.g. [1, 5, 8, 9, 21]), allows for the comparison of ideal and non-ideal effects in the VLE description of different mixtures.

To evaluate the performance of the implemented VLE approaches, Fig. A.3 shows the boiling-point diagram of three selected mixtures at atmospheric pressure, which are further analyzed in section 4. The selected mixtures refer to typical fuel mixtures, namely n-hexadecane/n-heptane, ethanol/iso-octane, and ethanol/water (hydrous ethanol). This specific choice was also made to be comprehensive in terms of the generality of mixture polarities - herein, we analyze all possible combinations: non-polar + non-polar (NN), polar + non-polar (PN), and finally polar + polar (PP).

The results presented in Fig. A.3 gradually evolve in terms of the complexity associated with the interactions between components. The vapor-liquid equilibrium for the alkane mixture (Fig. A.3(a)) is relatively simple, even though n-heptane is considerably more volatile than n-hexadecane. Differences between Raoult's law and the UNIFAC method are minor, which is expected for most combinations of n-alkanes under atmospheric pressure [31].

In contrast to the alkane mixture, both the ethanol/iso-octane and the ethanol/water mixtures feature strong non-ideal behaviors - this is illustrated by the difference between the ideal formulation (Raoult's law) and a non-ideal formulation (here applied through the UNIFAC method). Both also exhibit an azeotrope point, wherein the composition of the vapor phase is indistinguishable from the composition of the gas phase.

When comparing results presented in Fig. A.3(b) and Fig. A.3(c) with experimental data, a good agreement can be noticed. This successfully validates the implemented UNIFAC procedure to describe the VLE.

2.6. Summary of model key elements

Within the derivation process, focus has been given on a comprehensive description of the main underlying phenomena to the droplet heat and mass transfer, while combining theoretical elements well-known from the literature into a useful and workable framework. Single droplets evaporating in homogeneous atmospheres are considered to better isolate the main processes related to multi-component droplet heat and mass transfer. In this sense, the characteristics and limitations of the proposed model can be assessed prior to analysis accounting for more complex phenomena.

Considering the above, differential diffusion effects are accounted for in species and energy transport equations. As shown in this section and in the supplementary material, the heat and mass transfer equations in our proposed model are coupled in key steps of the analytical derivation. In the next section, it is also shown that this is also true for the numerical solution of the resulting system of equations. The developed coupled procedure contrasts with other solution strategies, wherein mass transfer rate is solved in an isolated framework prior to the heat transfer rate, e.g. as done in [7]. Also, throughout the derivation, no ad-hoc assumption is made to limit the heat and mass transfer process to evaporation or condensation mechanisms over the droplet lifetime. Finally, due to the absolute value operator that arises from the integration procedure (e.g., as in Eq. 5), the range of validity of the model is extended. In other models, the absence of the absolute operator does not allow for the calculation to proceed when the argument of the logarithm operator is negative.

3. Solution strategy

Regarding the proposed modeling, two aspects require special attention to address droplet heat and mass transfer in general ambient compositions. One concerns the absolute operator, while the other refers to the consideration of the fractional evaporation rate of species k (ε_k).

The discontinuous behavior of the absolute operator enforces that the solution must proceed in different ways according to the arguments of this operator. This choice, in turn, requires some arbitrariness regarding solver implementation, as floating-point operations are considered. This aspect was the main motivation for using a coupled procedure to solve the derived equations.

Within this procedure, Eqs. 19-21 and the continuity equation build up a system of non-linear equations which is solved at once instead of solving each equation individually (i.e. uncoupled solver). As a result, the mentioned arbitrariness are resumed to those intrinsic to the non-linear system solver of choice.

Regarding the consideration of ε_k in the equation set presented in section 2, this imposes an additional challenge for the solution algorithm: division by zero when $\dot{m} = 0$. Such a condition has a different interpretation in the context of multi-component liquids when compared to the single component counterpart. In this case, $\dot{m} = \sum_k \dot{m}_k = 0$ does not necessarily mean that all \dot{m}_k are zero, but rather, that they can have different, compensating contributions of evaporation/condensation. To overcome this issue, the so-called m -based approach has been derived, wherein the ε_k are expressed in terms of their definition \dot{m}_k/\dot{m} in all equations of Sec. 2. Such a strategy is of fundamental importance for a robust method capable of describing phase change in general atmosphere compositions. In analogy with the m -based approach, the strategy of expressing the equations set in terms of ε_k are referred as the ε -based approach. More details about the derivations of both approaches are found in the supplementary material of this manuscript.

As the m -based approach is more robust than the ε -based one (see section 5), the m -based is adopted as the main solution strategy in the present manuscript. Except when explicitly mentioned, this strategy is the one employed in our investigations. The remainder of this section focuses in the m -based approach as well, since the achievement of the corresponding equations for the ε -based approach is straightforward.

Within the m -based approach, the following set of equations is considered.

$$\dot{m}_k = \frac{\dot{m} \left(Y_k^s - \delta_{\dot{m}_k}^{\text{abs}} Y_k^\infty \zeta_{\dot{m}_k} \right)}{1 - \delta_{\dot{m}_k}^{\text{abs}} \zeta_{\dot{m}_k}}; \quad \text{if } \frac{\dot{m}_k - \dot{m} Y_k^\infty}{\dot{m}_k - \dot{m} Y_k^s} > 0 \quad \delta_{\dot{m}_k}^{\text{abs}} = 1, \quad \text{else } \delta_{\dot{m}_k}^{\text{abs}} = -1 \quad (19)$$

$$\dot{q}_d = \frac{\sum_k \dot{m}_k c_{p,k} (T^\infty - T^s)}{\delta_{\dot{q}_d}^{\text{abs}} \zeta_{\dot{q}_d} - 1} - \sum_k \dot{m}_k L_k; \quad \text{if } (1 + B_T) > 0 \quad \delta_{\dot{q}_d}^{\text{abs}} = 1, \quad \text{else } \delta_{\dot{q}_d}^{\text{abs}} = -1, \quad (20)$$

where

$$\zeta_{\dot{m}_k} = \exp \left[\frac{\dot{m}}{4\pi R_d \rho D_{k,m}} \right], \quad \zeta_{\dot{q}_d} = \exp \left[\frac{\sum_k \dot{m}_k c_{p,k}}{4\pi R_d \lambda} \right], \quad (21)$$

with B_T expressed in terms of \dot{m}_k on Eq. 7. Finally, the global mass conservation closes the equation set, namely $\dot{m} = \sum_k \dot{m}_k$.

Regarding the absolute operator in the equations of heat and components mass transfer rates, two expressions for each one of these transfer rates are implemented as seen in Eqs. 19-20. At each time step, a check is made to determine which expression will be chosen by the solver in agreement with the argument value of the absolute operator. Here, this procedure is encapsulated through the δ unitary variables.

Following this equation set, the problem is therefore well defined, by having $k + 2$ equations for $k + 2$ variables to be determined (all \dot{m}_k , \dot{m} , and \dot{q}_d). The system of non-linear equations is then solved at each time step in a dedicated numerical code written in Python. To accomplish the solution of the non-linear system, the Scipy library is considered, more specifically the Optimize module through the function fsolve [32]. This function is a wrapper around MINPACK's hybrid function [33] which itself is a modification of the Powell method [34]. This function operates trying to find zeroes to residual expressions, i.e. the solver is fed with guesses (superscript G below) expected to be close to the actual converged values which lead to residuals \mathcal{R} obtained at each time step:

$$\dot{m}_k^G - \frac{\dot{m}^G \left(Y_k^s - \delta_{\dot{m}_k^G}^{\text{abs}} Y_k^\infty \zeta_{\dot{m}_k^G} \right)}{1 - \delta_{\dot{m}_k^G}^{\text{abs}} \zeta_{\dot{m}_k^G}} = \mathcal{R}_{\dot{m}_k}; \quad \text{if } \frac{\dot{m}_k^G - \dot{m}^G Y_k^\infty}{\dot{m}_k^G - \dot{m}^G Y_k^s} > 0 \quad \delta_{\dot{m}_k^G}^{\text{abs}} = 1, \quad \text{else } \delta_{\dot{m}_k^G}^{\text{abs}} = -1, \quad (22)$$

$$\dot{q}_d^G - \frac{\sum_k \dot{m}_k^G c_{p,k} (T^\infty - T^s)}{\delta_{\dot{q}_d^G}^{\text{abs}} \zeta_{\dot{q}_d^G} - 1} + \sum_k \dot{m}_k^G L_k = \mathcal{R}_{\dot{q}_d}; \quad \text{if } (1 + B_T^G) > 0 \quad \delta_{\dot{q}_d^G}^{\text{abs}} = 1, \quad \text{else } \delta_{\dot{q}_d^G}^{\text{abs}} = -1, \quad (23)$$

3.1. Initialization

The initial guesses are described here. The global evaporation rate is computed by

$$\dot{m}^{\text{init}} = 4\pi R_d \rho \bar{D} \ln(1 + B_M), \quad (24)$$

where the superscript init stands for a guess used only at the initialization. Note that, at initialization, the result of a preferential diffusion problem is assumed to allow for the computation of the global evaporation rate. The averaged Spalding mass transfer number is also employed, i.e. Eq. 12. The average diffusion coefficient \bar{D} on Eq. 24 is computed in the same manner as in [7], namely

$$\bar{D} = \frac{\sum_{\text{vapor}} Y_k^{\text{ref}} D_k}{\sum_{\text{vapor}} Y_k^{\text{ref}}}, \quad (25)$$

in which Y_k^{ref} is the reference mass fraction inside the film region for each species k . Notice however that the summations are carried out ignoring all inert species. In this work, the computation of Y_k^{ref} follows the one-third rule between mass fractions on infinity and at the surface of the droplet, namely, $Y_k^{ref} = 1/3Y_k^\infty + 2/3Y_k^s$. Once the first global evaporation rate (Eq. 24) is computed, the evaporation rates of each individual species are abstracted from the definition of $B_{M,k}$, such that

$$\dot{m}_k^{init} = \dot{m}^{init} \left(Y_k^s + \frac{Y_k^s - Y_k^\infty}{B_M} \right) \quad (26)$$

Then, the assumption that $B_T = B_M$ is made for the purposes of initializing the heat entering the droplet (since B_T depends on \dot{q}_d which itself needs to be initialized):

$$\dot{q}_d^{init} = \frac{\sum_k \dot{m}_k^{init} c_{p,k} (T^\infty - T^s)}{\delta_{\dot{q}_d}^{abs,init} \zeta_{\dot{q}_d}^{init} - 1} - \sum_k \dot{m}_k^{init} L_k; \text{ if } (1 + B_M) > 0 \text{ } \delta_{\dot{q}_d}^{abs,init} = 1, \text{ else } \delta_{\dot{q}_d}^{abs,init} = -1, \quad (27)$$

Following this procedure, a first guess to \dot{m} , \dot{m}_k , and \dot{q}_d is computed. These values are then fed into the non-linear solver through Eqs. 22-23 which allow the simulation to start.

3.2. Further details

The time integration is performed using RK-23 or RK-45 Runge Kutta schemes throughout our analyses, both implemented inside the Scipy python module [32]. The results achieved from the initialization process are then used as guesses to start the first iteration. For the next iterations, the necessary guesses for the current iteration are chosen to be the converged results of the previous iteration. The convergence of the solver is controlled through an absolute tolerance for each variable as well as a relative tolerance applied to all variables.

To account for convective heat and mass transfer, Eq. 9 follows the same structure of the above solution strategy. Namely, the set of equations 19-20 but switching the ζ factors presented in both expressions in Eq. 21, respectively by

$$\zeta_{\dot{m}_k}^{conv} = \exp \left[\frac{\dot{m}}{4\pi R_d \rho D_{k,m}} \frac{1}{Sh_k} \right], \quad \text{and} \quad \zeta_{\dot{q}_d}^{conv} = \exp \left[\frac{\sum_k \dot{m}_k c_{p,k}}{4\pi R_d \lambda} \frac{1}{Nu} \right]. \quad (28)$$

4. Influence of the VLE approach

As previously mentioned, the Vapor-Liquid Equilibrium is a key aspect for the modeling of multi-component droplet heat and mass transfer. Therefore, it is the objective of this section to

evaluate the performance of the proposed modeling strategy combined with different VLE approaches.

In order to encompass a good representation of typical fuel mixtures, the vapor-liquid equilibrium approaches are analyzed for three binary mixtures of fuels: n-hexadecane/n-heptane, ethanol/iso-octane, and ethanol/water (hydrous ethanol). As discussed in section 2.5, these binary mixtures allow for the exploration of a general set of mixture polarities, i.e.: NN, PN, and PP. Simulations are conducted for droplets with initial diameters $d_0 = 50\mu\text{m}$, for varying initial volume fraction VF and initial temperatures. In a first moment, the surrounding gas temperature is set to be the same as the initial temperature of the droplet, namely $T_\infty = T_{d,0}$. Later on, an analysis is then conducted to see how these droplets behave at a high temperature environment. For both ethanol/water as well as ethanol/iso-octane droplets, initial temperatures are set at $T_{d,0} = 304\text{K}$. For the n-hexadecane/n-heptane droplets, different initial temperatures are used for each composition, as these are extracted from the experimental investigations conducted by Wilms [31]. Results follow in Figs. A.4 and A.5 for low temperature simulations. Then, a high temperature counterpart is presented in Fig. A.6 for the simulations of ethanol/water and ethanol/iso-octane droplets. Finally, a comparison is made in Fig. A.7 for the droplet composition evolution for both low and high temperature environments.

As expected from the boiling-point diagrams from Fig. A.3, there is no significant difference between Raoult's law and the UNIFAC method for n-hexadecane and n-heptane mixtures. Particularly, both depict a good agreement with the experimental data. The strong variation in diameter decay for the different initial conditions is well captured by the model. Such a performance demonstrates the good coupling between heat and species mass transfer rates achieved with the proposed model.

Despite not being shown here, a good agreement with the experimental data presented in [31] could also be observed for n-tetradecane and n-hexadecane mixtures, as achieved in [21] where the model proposed in [7] was applied. Results of a n-hexadecane and n-heptane mixture were preferred however as the volatility of the two components differ greatly. Such a characteristic allows a better evaluation of the robustness of the proposed model. Furthermore, for the next simulated cases, high volatile species have always been considered.

No differences between Raoult's law and the UNIFAC method are visible at the extremes of the analyzed composition ranges for ethanol/iso-octane (Fig. A.5 top) and ethanol/water (Fig. A.5 bottom) mixtures. In such extreme compositions, droplets are single-component and both VLE methods behave similarly. However, for intermediary compositions, great differences can be spotted on the behavior of the evaporative process, even though the predicted droplet lifetime is nearly the same. For the ethanol/iso-octane case, there is also considerable difference in the predicted temperature at the end of the droplet lifetime. Differences in the prediction of droplet temperatures for ethanol/water mixtures do also occur, but not as pronounced as for ethanol/iso-octane mixtures. Such an outcome indicates the strong coupling between heat and species mass transfer rates and the VLE approaches.

Fang et al. [8] conducted a study wherein the evaporation model developed by Brenn et al. [5] was extended to include thermal radiation effects as well as a non-ideal description of the vapor-liquid equilibrium closure through the UNIFAC method. They reported that for high temperatures the inclusion of a non-ideal description was found to be less important when compared to lower temperatures. Such results motivated the realization of similar simulations in the present work⁵ as those presented in Fig. A.5. For this analysis, the surrounding gas temperature of $T_\infty = 703K$ is adopted in accordance with [8]; results follow in Fig. A.6.

The difference between the ideal and the non-ideal approach tends to be lessened for the evolution of the normalized droplet's surface, as presented in Fig. A.6. This result is in accordance with what was reported in [8]. However, when looking at the droplet temperature evolution, there is clearly a difference on the transient behavior, which can even be greater than the one observed in the low temperature case. Typically, results for the non-ideal approach tend to quickly converge to a temperature plateau, whereas the ideal counterpart leads to a more continuous evolution over time, later stabilizing at a higher temperature. In some cases, it is possible to see a spike in temperature towards the end of the droplet lifetime for non-ideal approaches, and when this is captured, the final temperature tends to be the same as the one predicted by the ideal approach.

Based on the differences noticed for the droplet temperature, impacts of the VLE approach

⁵As we do not account for radiation in our methodology, it is not relevant to perform comparison between our simulation and the ones in [8]

on the liquid composition are analyzed. Results follow in Fig. A.7 for simulations conducted at low and high ambient temperatures. Note that mass fractions have been normalized to improve data visualization as the initial composition of the different cases is not the same. Results for pure substances are not included in Fig. A.7, as they depict no internal composition variations during the droplet lifetime in these simulations.

As seen in Fig. A.7, results can drastically vary depending on whether an ideal or non-ideal description of the VLE is chosen. Such an outcome is noticed for both low and high temperature scenarios. In some cases, the normalized mass fraction of ethanol tends to increase when using non-ideal approaches (droplet tends to become pure ethanol as it evaporates, $Y_{d,Eth}/Y_{d,0,Eth}$ increases) whereas the ideal counterpart leads to the inverse behavior. This is discussed in more detail in section 6. Still, for CFD applications it is important to correctly predict mass source terms for each fuel species and therefore the correct VLE approach should be picked accordingly.

The results presented in this section reinforce the main outcomes obtained in a previous study [21], where simulations were conducted with the Tonini and Cossali [7] model and the same UNIFAC algorithm as used here. Indeed, Raoult's law is insufficient to describe the VLE of non-ideal liquid mixtures, which is reflected in the prediction of typical droplet evaporation-related metrics. Nevertheless, in the results presented in this section, both tested VLE approaches deliver similar droplet lifetimes, which may be an important indicative for investigations on real sprays. For instance, comparisons between spray penetration lengths may be insufficient to evaluate if a multi-component spray is well predicted by a CFD model based on the ideal VLE approach. Perhaps, droplet size distribution acquired throughout the spray flow may prove to be useful to address such an issue.

5. Droplet heat and mass transfer in atmospheres with high vapor concentration

As mentioned in the introduction of this manuscript, the consideration of combustion processes for hydrophilic fuels in spray flows imposes a quite challenging scenario: droplet heat and mass transfer in atmospheres with high mass fractions of a liquid vapor species. Such a challenging scenario is not specific to the combustion of liquid hydrophilic fuels, but may also occur in any flow where liquid droplets interact with atmospheres composed of varying vapor mass fractions

crossing the saturation values defined by the droplet surface temperature and the ambient pressure. In a more pragmatic viewpoint, such operating conditions impose a stress point that leads other formulations to fail, while the current model proposition succeeds. In this section, the investigation of such operating conditions follows the study conducted by Law et al. [35], where droplets of liquid methanol (hydrophilic fuel) interact with air atmospheres at different relative humidity values. Afterwards, models are tested in more severe conditions which seek to mimic the interaction of hydrophilic fuel droplets with freely propagating laminar flames.

Single droplet evaporation cases in quiescent atmospheres are conducted with pure methanol, in which the initial diameter is set to $d_0 = 1.6\text{mm}$, and both liquid and air temperatures are $T_{d,0} = T_\infty = 298\text{K}$. A first case is defined for zero relative humidity ($\phi = 0$) and then a second one for the maximum relative humidity ($\phi = 1.0$) at this temperature. For each simulation, three different implementations, namely, both the m -based and the ε -based approaches of the proposed model, and the formulation present in [7], are compared with results extracted from [35]. Particularly, the model proposed by Tonini and Cossali [7] is used as a reference in the present work as previously done in [21]. Results are displayed in Fig. A.8.

As seen in Fig. A.8 (top), there is no difference between all three formulations for the dry air case ($\phi = 0$). This is somewhat expected since the droplet stays single-component throughout its lifetime, with initial conditions that ensure only evaporation occurs (no condensation). However, for the case with maximum relative humidity, the formulation as presented by Tonini and Cossali [7] detaches itself from the two other formulations, predicting a lower temperature which translates into a slower evaporation rate. There may be many reasons to explain this different behavior, including for example the different solution strategies as explored in section 3 and the novel energy formulation, since the model of Tonini and Cossali [7] follows the one developed by Abramzon and Sirignano [11]. Similarly, the clear differences among modeling strategies may justify the deviations observed between the results obtained with the model proposed by Law et al. [35] and the other ones.

It has to be mentioned that none of the simulations conducted here includes the heat transfer process through the support fiber that holds droplets in the experimental apparatus. The inclusion of such an effect is supposed to increase the evaporation rates and to reduce the deviations noticed

among simulation results and experimental data [36]. To showcase more validation data to support the current model proposition, the reader can find in Appendix 9 a comparison with experimental and numerical data from [37] for the evaporation of ethanol/water droplets in atmospheres composed of high relative humidity. Therein, a good agreement is also found between our results and the experimental data reported. Even though some deviations are noticed in specific scenarios, those are similar to those observed in their numerical results.

In agreement with the previous tests, a pure methanol droplet is used to stress the chosen modeling strategies in more severe conditions. A droplet of initial diameter $d_0 = 20\mu\text{m}$ is injected with initial temperature $T_{d,0} = 300\text{K}$ into an atmosphere of the same temperature, $T_\infty = 300\text{K}$. However, this droplet was injected with velocity $U_{d,0} = 0.5\text{m/s}$ into an atmosphere with a bulk velocity of $U_\infty = 0.5\text{m/s}$ such that no drag effects are present even though the droplet is moving. This droplet moves through a first zone of length $L_0 = 0.5\text{cm}$ to then meet the representation of a flame-front, here described through a hyperbolic tangent profile rising from a temperature of $T_\infty = 300\text{K}$ to approximately $T_\infty = 2000\text{K}$ and a water composition at infinity rising from $Y_{\infty,\text{Wat}} = 0$ to approximately $Y_{\infty,\text{Wat}} = 0.15$. These atmospheric conditions aim to represent a freely propagating one-dimensional flame of general hydrocarbons where the mass fraction profile of water reaches the maximum value of a stoichiometric combustion reaction of methanol in air. The length of the region defined by the hyperbolic tangent profile is set to be $L_{\text{flame}} = 0.1\text{mm}$, in view of the representation of a general hydrocarbon flame thickness. Results follow in Fig. A.9.

In Fig. A.9, the robustness of the m -based approach of the proposed model is clearly demonstrated, as this is the only approach able to carry the simulation until the end of the droplet lifetime. Moreover, all three formulations perform in practically identical fashion up until other formulations stop working. The first formulation to fail is the one of Tonini and Cossali [7], because the droplet enters in a regime for which the absolute value is necessary to proceed with the simulation. After some time inside this regime, the ε -based approach fails. This limitation occurs because the droplet temporarily starts to condensate - therefore, passing the singular point of $\dot{m} = 0$ wherein any fractional evaporation rate ε is mathematically undefined. Therefore, it is possible to see that the m -based approach is able to handle cases in which a droplet evaporates, then condensates and then evaporates again, with parameters varying in a steep manner as representative of combustion

process for hydrophilic fuels.

6. Importance of differential diffusion modeling

If differential diffusion effects are accounted for, the evaporation preference of the participating liquid species does not follow the predicted behavior by simplified approaches. Hereafter, we refer to such a behavior as the inversion problem. The inversion of the evaporation preference of vapor species in multi-component droplets have been noticed for instance in [38], where a comprehensive investigation is carried out in terms of the so-called separation factor. In that work, it could be noticed that the inversion problem was triggered by the consideration of ideal and non-ideal VLE approaches. Nevertheless, in [38] such an investigation was limited to the VLE modeling as no differential diffusion was accounted for. Following the present analysis, which does not intend to be exhaustive in the topic, the inversion problem is limited to mixtures where nonpolar substances and non-ideal VLE approaches are considered. It should be noted however that this behavior seems to be universal to differential diffusion formulations, since the inversion phenomena can also be observed when employing the procedure proposed by [7] as well, as shown in this section.

Figure A.10 (top) illustrates the inversion problem in terms of the normalized droplet surface area and internal mixture composition for a ethanol/water binary mixture. Simulations are conducted for droplets of initial diameter $d_0 = 20\mu m$, the same initial temperature as the gas in the far field $T_{d,0} = T_\infty = 300K$, and an initial composition of $VF_{\text{ethanol}} = 0.95$. For all simulations, the non-ideal VLE was characterized through the UNIFAC formulation. The relative air humidity is set to $\phi = 0$.

Two models constructed in a differential diffusion (DD) framework (the model proposed here and the one presented in [7]) are compared with a simplified formulation of the m -based approach within a preferential diffusion (PD) framework. To achieve the preferential diffusion scenario, instead of using a diffusion coefficient for each species, a global, average diffusion coefficient is applied (i.e. Eq. 25). To compute this global coefficient, the diffusion coefficients D_k are computed with the same formulation as in [7]. Also noteworthy is that, the index k in Eq. 25 only scans through the vapor species, with inert species not taken into account, such that $\sum_{k=1}^N Y_k^{ref} < 1.0$ for instance. Therefore, the diffusion coefficient computed for the preferential diffusion approach

through Eq. 25 represents a case in which all liquid species can be clumped together as a single vapor diffusing in binary fashion towards a single, clumped inert species.

The three compared approaches depict similar results for the evolution of the normalized droplet surface area. However, differences in the droplet internal composition are clear with the treatment given to the diffusive transport of species. In both models based on the DD approach, water leaves the droplet first, delivering a pure ethanol droplet at the end of the evaporation process. On the other hand, when the PD approach is accounted for, ethanol leaves the droplet at first despite composing 95% of the initial volume fraction of the liquid.

The behavior observed with the PD approach sounds intuitive due to the highest volatility of ethanol when compared with water. Nevertheless, bearing in mind that the diffusive transport is decisive to define the mass transfer in an evaporating droplet (as such a phenomenon define the so-called hydrodynamic evaporation models [15]), another aspect competes with the component volatility: the diffusion coefficient D_k . The diffusion coefficients of water are larger than those of ethanol as seen in Fig. A.2. Such a characteristic implies that water molecules can travel faster than ethanol molecules in air, allowing a higher flux of water away from the droplet surface.

During the development of our investigations, we also observed that different modeling strategies for the computation of the non-ideal VLE, the binary and multi-component diffusion coefficients affect the condition in which the inversion problem is triggered. Nevertheless, such an influence is small, and for our simulations, no combination of these models was able to inhibit this effect. Considering these aspects, some investigations are conducted in order to evaluate the influence of specific variables on the triggering of the inversion problem. Specifically, the vapor concentration in the far field demonstrated to be a key parameter in this issue. Hence, the influence of the air humidity is investigated in the sequel.

Simulations follow the same ambient conditions applied to the case presented in Fig. A.10(top), i.e. ethanol/water droplets with $d_0 = 20\mu\text{m}$, $T_{d,0} = T_\infty = 300\text{K}$, and $VF_{\text{ethanol}} = 0.95$. The relative air humidity is increased and Fig. A.10(bottom) showcases the results for $\phi = 0.4$, through the normalized droplet surface area and the internal composition of the droplet.

As seen in Fig. A.10, as the relative humidity is increased, differences in the prediction of the droplet lifetime start to become more apparent between the different models. Also, the behavior in

predicting the internal composition evolution can be quite different. Along with the development of this study, various tests have been conducted varying the relative humidity. From these investigations it could be noticed that the inversion problem ceases as long as the relative humidity is higher than $\phi \approx 0.025$ for $T_\infty = 300K$. From this value of relative humidity, the behavior shifts towards those presented in Fig. A.10 (bottom), that is, ethanol evaporates first, leaving a single-component water droplet characterized by a slower evaporation rate and the change in the slope of the normalized surface curve.

It is important to analyze if this inversion effect is still present in the same manner for high temperature environments, as indicated in section 4. To analyze this, similar simulations to those presented in Fig. A.10 were ran but this time imposing a surrounding gas temperature of $T_\infty = 703K$. Of note is the fact that, at this temperature, the notion of relative humidity is no longer as useful since water could exist at any concentration in the gas phase. Therefore, the analysis is shifted towards molar fractions at infinity. Results showed that (not presented here), at this high temperature the inversion behavior was present up to molar fractions of $X_{\infty, Wat} \approx 0.010$; for the low temperature case, a relative humidity of $\phi = 0.025$ corresponds roughly to $X_{\infty, Wat} \approx 0.002$. Therefore, the inversion phenomenon is observed for vapor mass fractions of approximately 5 times greater than the values achieved for the low temperature counterpart. For temperatures up to 2000K, the inversion phenomenon was observed for mass fractions up to $X_{\infty, Wat} \approx 0.023$, i.e. ten times greater than the results reported for low temperatures. These results suggest that preferential evaporation and the vapor-liquid equilibrium at the interface can still be relevant at high temperatures, extending the findings reported by Fang et al. [8].

From the results presented in Fig. A.10 it is clearly noticed that the choice of the diffusion transport approach does interfere with the heat and mass transfer processes in a droplet. Following the specific approach of choice and the surrounding gas compositions, the sequence that the vapor of a specific component is released from the droplet surface is defined. Such an outcome requires a special care for CFD simulations of multi-component sprays, where dry air is typically employed as the carrier gas. In particular to combustion applications, the order in which a species is released from the droplet may affect the mixture preparation process and, consequently, the evolution of chemical reactions. Nevertheless, as soon as more realistic air compositions are considered, which

account for air humidity, problems should be attenuated when multi-component droplet models based on differential-diffusion are applied.

6.1. Influences of multi-component diffusion coefficient approaches

The existence of different possibilities to address the multi-component diffusion coefficient D_k claims to investigate the influence of these possibilities on the computation of heat and mass transfer of multi-component droplets. Given this, the different approaches presented in section 2.4 to estimate the multi-component diffusion coefficient are tested in this section. Herein, only the proposed model following the m -based approach is considered.

Altogether two approaches are analyzed, Blanc's law as given by Eq. 16 and the one proposed by Coffee and Heimerl [26]. Initially, simulations were ran for the exact same ethanol/water test cases presented in Fig. A.10; however, no notable differences were spotted between both approaches. Deviations between both approaches become noticeable when the temperature of the surrounding gas and the vapor mass fraction of water were increased, resembling conditions more representative of droplets interacting with flames.

Figure A.11 presents the evolution of the liquid components mass fractions and the temperature of droplets in quiescent atmospheres at $T_\infty = 1500K$ and with water vapor mass fractions of 0.0 and 0.1, respectively. In both figures, deviations between both tested approaches can be noticed.

As seen in Fig. A.11, for a high-temperature environment, both formulations can not only showcase differences in the transitory behavior of the droplet evaporation, but also notably on the maximum temperature of the droplet. This behavior can be justified by the different values of the multi-component diffusion coefficients delivered by each approach, which are directly connected with the main driven mechanism for the mass transfer process. Changes on the liquid temperature are associated with the clear coupling between heat and mass transfer processes, which is strongly valued throughout the derivation and solution process of the proposed approach.

In fact, the noticed modification on liquid composition and temperature indicates that the choice for a specific model to represent the multi-component diffusion coefficient affects the exchange rates of heat and component masses between both phases. Consequently, this may interfere with CFD predictions of multi-component spray flows in high temperature atmospheres. However,

it is necessary to highlight that, in contrast to the consideration of differential diffusion effects, such differences are limited to a specific range of gas temperature and vapor mass fractions. Subsequent works are planned to investigate the influence of different approaches of the multi-component diffusion coefficients for the prediction of multi-component heat and mass transfer in more details.

7. Model performance in convective heat and mass transfer

Special attention is paid to the influence of taking or not taking into account the correction factor for Stefan flow effects for convective heat and mass transfer, showcased in Eqs. 13 and 14. This comparison was motivated by the limitations of correction factors based on the film theory for strictly positive values of the Spalding numbers, as previously discussed in section 2.3. It is important to highlight that, the proposed formulation of this work manages to take into account cases wherein Spalding numbers can become negative, thus invalidating the wide use of such correction factors. Regardless of the subsequent results, the present discussion exposes a need for more general Nusselt and Sherwood correlations specific to multi-component droplets. Particularly, correlations that are able to take into account varying states between evaporation and condensation during the lifetime of a single droplet, corresponding to outward and inward Stefan flow respectively inside the film region.

Within the solution strategy adopted for the proposed model (see section 3), the influence of the convective heat and mass transfer processes is expressed in terms of the ζ^{conv} factors as defined by both expressions in Eq. 28. As Nusselt and Sherwood numbers are inside the ζ factors, this specific approach is labeled here *in-exp*. This approach contrasts for instance with the procedure described on Tonini and Cossali [7], where the authors have opted to describe the convective influence as a multiplicative factor outside of the exponential, in analogy with the single-component results obtained from Abramzon and Sirignano [11]. The effects of such an approach are also investigated here under the label *out-exp* but within the proposed model framework.

Simulation results were compared to the experimental data presented in ([39, 40]) for ethanol/water droplets with varying initial compositions represented in terms of mass fractions. In agreement with the experimental measurements, the initial droplet diameter is $d_0 = 1.2mm$, the initial droplet

temperature is $T_{d,0} = 293.15K$ and the surrounding gas temperature is $T_{\infty} = 400K$. The droplet is exposed to a free-flow with fixed velocity $U_{\infty} = 2m/s$.

In Fig A.12, deviations between results with and without the correction of Stefan flow effects are not expressive in all of the tested cases. However, an appreciable difference is found when comparing the two approaches used to incorporate convection effects in the proposed model. Results achieved for the *in-exp* approach deliver slightly higher evaporation rates than the *out-exp* in all simulated conditions. Such a behavior allows a slightly better agreement with the experimental data for pure components, while the opposite occurs for intermediary compositions. Nevertheless, both approaches present a general good agreement with the experimental data.

It is important to mention that dry air has been considered in all simulations while experimental tests have been conducted with atmospheric air, which may present some humidity. The presence of water vapor in the surrounding gas may contribute to a delay in the evaporation rate as the mass transfer potential for water (i.e. the Spalding number associated with this component - B_{H_2O}) reduces. Also, the slope of the normalized droplet surface area may change with the consideration of some relative humidity. Both aspects are observed in the results presented in sections 5-6, which may allow a better agreement with the chosen experimental data.

8. Summary and conclusions

This paper proposes a novel modeling approach to describe heat and mass transfer for multi-component droplets immersed in general atmosphere compositions. The model is derived from general energy and species transport equations, including differential diffusion effects in terms of Fick's law. The paper describes specific modeling steps and required simplifications. Our analyses tested the influence of specific variables, properties, and formulations. Although simulations were conducted for binary liquid mixtures, the proposed model has no theoretical restrictions to simulate mixtures with more than two compounds. Various scenarios were considered to evaluate the specific modeling aspects. These scenarios were based on either experiments or artificial albeit realistic situations.

Investigations conducted with different binary mixtures demonstrated that the model has no restriction to run with different VLE approaches and combinations of component polarities. Within

the analysis of the VLE approaches, the model has been validated for mixtures of non-polar liquids exhibiting different volatilities. Particularly, throughout the manuscript, substance pairs of different volatilities prevail in order to stress the model. The comparisons of different VLE behavior associated with specific substance pairs showcase that deviations noticed in boiling point diagrams between both tested VLE approaches are reflected in typical metrics applied to analyse droplet heat and mass transfer. Particularly, alkane mixtures demonstrated to be insensitive to the considerations of the non-ideal VLE approach, while such an approach was necessary to describe other mixture pairs.

Special attention has been paid to the representation of the droplet heat and mass transfer process at severe atmosphere conditions. Specifically, this was one of the main motivations for deriving the proposed model. Two kinds of tests have been used to evaluate the model robustness and the behavior of different solution strategies. The first considered comparisons with experimental data, in which methanol droplets (i.e. a hydrophilic substance with high volatility) evaporate in dry and humid air. In this framework, all of the employed models could manage to address the problem. All of them showcase a good agreement with reference experimental data and numerical predictions. Such a good agreement was more pronounced for the more severe condition, where the relative humidity is set to 100%. In view of combustion applications, an artificial test case is employed where the interaction of binary mixtures composed of reactants and products species with a freely propagating flame is emulated. Therein, the robustness of the proposed model and the limitations of other two modeling strategies could be clearly pointed out. As soon as evaporating droplets start to interact with high temperature regions which also possess high mass fractions of vapor, typical approaches fail. This is because of specific mathematical limitations. Nevertheless, the combination of the derived mathematical equations and the proposed solution strategy, the proposed model has no restrictions to address such challenges.

As the entire derivation process relies on considering differential diffusion effects, a section is specifically dedicated to pointing out the importance of such modeling aspect for multi-component droplets. Two other issues are thoroughly discussed in this context: the calculation of multi-component and binary diffusion coefficients. Such an analysis was motivated by the perception of the inversion of the order that substances are released from the droplet surface when considering

differential diffusion and non-ideal VLE approaches. As mentioned, such a behavior is not a particular characteristic of the proposed model, but it occurs with other models available in the literature as well. From the conducted analysis, it turns out that when multi-component droplet heat and mass transfer models based on differential diffusion are considered, the air humidity must be accounted for. Further investigations showcase that the choice for a specific model to address the diffusion coefficient and the consideration of differential diffusion impacts the evolution of droplet heat and mass transfer processes. The assessment of different approaches used to address the species diffusion transport into the gas phase, which includes investigations of the impact of different multicomponent diffusion coefficient models, will be subject of future works.

Finally, convective droplet heat and mass transfer are considered for different mixtures of ethanol and water. Comparisons with experimental data successfully validated the proposed model. Altogether four modeling strategies have been tested, allowing to explore all the combinations resulting from the variation of two parameters: Stefan flow correction and the embedded solution of convective effects. The correction of the Nusselt and Sherwood numbers due to the Stefan flow effects was not expressive in the simulated cases. Therefore, the more general solution demonstrated to be sufficient for the tested scenarios. However, further investigations about the possibility to include negative values of the Spalding numbers in the corresponding equations of the film theory are encouraged. This is expected to improve the accuracy of the model in such cases. In contrast to the insensitivity of the Stefan flow correction, the proposed model demonstrates to be affected by the possibility to embed Nusselt and Sherwood numbers in the resulting nonlinear system of the model than their consideration *a posteriori*. Although the results given by both approaches presented a good agreement with experimental data, the embedded solution is recommended since it is more coherent with the coupled solution strategy adopted throughout this study.

As a perspective, the proposed single droplet model can be used for the simulation of dilute sprays in non-reacting and reacting conditions (without isolated droplet combustion), using the so-called Particle-Source-In Cell (PSI-CELL) approach [41]. This strategy does not differ from that applied in [42] for multi-component non reacting spray flows, or for instance in [43] and [44] for single-component turbulent spray flames.

9. Acknowledgements

We acknowledge the financial support from São Paulo Research Foundation (FAPESP - grants # 17/06815-7 and # 18/03849-0). Support from the French Agence Nationale de la Recherche in the MIMETYC project (grant ANR-17-CE22-0003) is also acknowledged.

Appendix A. Ethanol-Water droplet evaporation validation for high relative humidities

In Fig A.13, results from current model proposition are showcased against experimental data and a numerical model from [37]. As explained from the authors of that study, deviations between experimental and numerical results may stem from uncertainties regarding initial droplet concentration determination, exact initial droplet size and measurements regarding relative humidity. Still, a good agreement was found overall. Initial radii for simulations were extracted from the original plots, and were input as follows: $r_{d,0} = 22\mu\text{m}, 20.8\mu\text{m}, 21.7\mu\text{m}, 20.8\mu\text{m}$ for relative humidities of $\phi = 0.58, 0.77, 0.87, 0.91$ respectively.

References

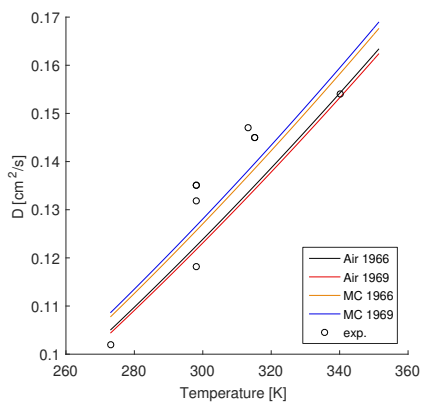
- [1] A. Millán-Merino, E. Fernández-Tarrazo, M. Sánchez-Sanz, Theoretical and numerical analysis of the evaporation of mono- and multicomponent single fuel droplets, *Journal of Fluid Mechanics* 910 (2021).
- [2] R. S. Miller, K. Harstad, J. Bellan, Evaluation of equilibrium and non-equilibrium evaporation models for many-droplet gas-liquid flow simulations, *International Journal of Multiphase Flow* 24 (1998) 1025–1055.
- [3] W. A. Sirignano, *Fluid Dynamics and transport of droplets and sprays*, 2nd ed., Cambridge University Press, New York, NY, 2010.
- [4] F. L. Sacomano Filho, G. C. Krieger Filho, J. A. van Oijen, A. Sadiki, J. Janicka, A novel strategy to accurately represent the carrier gas properties of droplets evaporating in a combustion environment, *International Journal of Heat and Mass Transfer* 137 (2019) 1141–1153.
- [5] G. Brenn, L. J. Deviprasath, F. Durst, C. Fink, Evaporation of acoustically levitated multi-component liquid droplets, *International Journal of Heat and Mass Transfer* 50 (2007) 5073–5086.
- [6] V. Ebrahimian, C. Habchi, Towards a predictive evaporation model for multi-component hydrocarbon droplets at all pressure conditions, *International Journal of Heat and Mass Transfer* 54 (2011) 3552–3565.
- [7] S. Tonini, G. E. Cossali, A novel formulation of multi-component drop evaporation models for spray applications, *International Journal of Thermal Sciences* 89 (2015) 245–253.

- [8] B. Fang, L. Chen, G. Li, L. Wang, Multi-component droplet evaporation model incorporating the effects of non-ideality and thermal radiation, *International Journal of Heat and Mass Transfer* 136 (2019) 962–971.
- [9] P. Narasu, S. Boschmann, P. Pöschko, F. Zhao, E. Gutheil, Modeling and Simulation of Single Ethanol/Water Droplet Evaporation in Dry and Humid Air, *Combustion Science and Technology* 192 (2020) 1233–1252.
- [10] L. Zhang, S. C. Kong, Multicomponent vaporization modeling of bio-oil and its mixtures with other fuels, *Fuel* 95 (2012) 471–480.
- [11] B. Abramzon, W. A. Sirignano, Droplet vaporization model for spray combustion calculations, *International Journal of Heat and Mass Transfer* 32 (1989) 1605–1618.
- [12] K. K. Kuo, *Principles of combustion*, 2 ed., John Wiley Sons Inc., 2005.
- [13] B. Somers, *The simulation of flat flames with detailed and reduced chemical models*, Ph.D. thesis, Technische Universiteit Eindhoven, 1994.
- [14] G. Lupo, C. Duwig, A Numerical Study of Ethanol-Water Droplet Evaporation, *Journal of Engineering for Gas Turbines and Power* 140 (2018) 21401.
- [15] S. S. Sazhin, Advanced models of fuel droplet heating and evaporation, *Progress in Energy and Combustion Science* 32 (2006) 162–214.
- [16] M. C. Yuen, L. W. Chen, On Drag of Evaporating Liquid Droplets, *Combustion Science and Technology* 14 (1976) 147–154.
- [17] F. A. Williams, *Combustion Theory*, (1985), 2 ed., Addison Wesley, 1985.
- [18] E. N. Fuller, P. D. Schettler, J. C. Giddings, A new method for prediction of binary gas-phase diffusion coefficients, *Industrial and Engineering Chemistry* 58 (1966) 18–27.
- [19] E. N. Fuller, K. Ensley, J. C. Giddings, Diffusion of halogenated hydrocarbons in helium. The effect of structure on collision cross sections, *Journal of Physical Chemistry* 73 (1969) 3679–3685.
- [20] I. V. Gnielinski, *VDI-Wärmeatlas, VDI Buch*, Springer Berlin Heidelberg, Berlin, Heidelberg, 2006.
- [21] A. C. Santos, A. Vié, F. L. Sacomano Filho, Modeling droplet evaporation of multi-component liquid fuel, in: *Proceedings of the European Combustion Meeting 2021*, Naples, Italy, 2021, p. 6.
- [22] K. K. Kuo, R. Acharya, *Fundamentals of turbulent and multiphase combustion*, 1 ed., John Wiley Sons Inc., Hoboken, New Jersey, 2012.
- [23] A. Blanc, Recherches sur les mobilités des ions dans les gaz, *Journal de Physique Théorique et Appliquée* 7 (1908) 825–839.
- [24] S. I. Sandler, E. A. Mason, Kinetic-theory deviations from blanc’s law of ion mobilities, *The Journal of Chemical Physics* 48 (1968) 2873–2875.
- [25] T. R. Marrero, E. A. Mason, Gaseous Diffusion Coefficients, *Journal of Physical and Chemical Reference Data* 1 (1972) 3–118.
- [26] T. P. Coffee, J. M. Heimerl, Transport algorithms for premixed, laminar steady-state flames, *Combustion and*

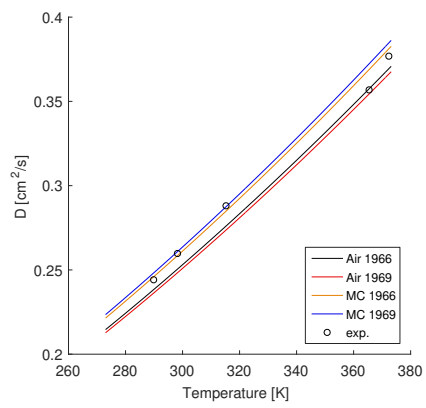
Flame 43 (1981) 273–289.

- [27] R. V. Mrazek, C. E. Wicks, K. N. S. Prabhu, Dependence of the Diffusion Coefficient on Composition in Binary Gaseous Systems, *Journal of Chemical and Engineering Data* 13 (1968) 508–510.
- [28] E. A. Mason, Higher approximations for the transport properties of binary gas mixtures. I. general formulas, *The Journal of Chemical Physics* 27 (1957) 75–84.
- [29] E. A. Mason, Higher approximations for the transport properties of binary gas mixtures. II. Applications, *The Journal of Chemical Physics* 27 (1957) 782–790.
- [30] B. E. Poling, J. M. Prausnitz, J. P. O’Connell, *The Properties of Gases and Liquids*, 5th ed., McGRAW-HILL, 2001.
- [31] J. Wilms, *Evaporation of Multicomponent Droplets*, Phd thesis, Universität Stuttgart, 2005.
- [32] P. Virtanen, R. Gommers, T. E. Oliphant, M. Haberland, T. Reddy, D. Cournapeau, E. Burovski, P. Peterson, W. Weckesser, J. Bright, S. J. van der Walt, M. Brett, J. Wilson, K. J. Millman, N. Mayorov, A. R. J. Nelson, E. Jones, R. Kern, E. Larson, C. J. Carey, Polat, Y. Feng, E. W. Moore, J. VanderPlas, D. Laxalde, J. Perktold, R. Cimrman, I. Henriksen, E. A. Quintero, C. R. Harris, A. M. Archibald, A. H. Ribeiro, F. Pedregosa, P. van Mulbregt, A. Vijaykumar, A. P. Bardelli, A. Rothberg, A. Hilboll, A. Kloeckner, A. Scopatz, A. Lee, A. Rokem, C. N. Woods, C. Fulton, C. Masson, C. Häggström, C. Fitzgerald, D. A. Nicholson, D. R. Hagen, D. V. Pasechnik, E. Olivetti, E. Martin, E. Wieser, F. Silva, F. Lenders, F. Wilhelm, G. Young, G. A. Price, G.-L. Ingold, G. E. Allen, G. R. Lee, H. Audren, I. Probst, J. P. Dietrich, J. Silterra, J. T. Webber, J. Slavič, J. Nothman, J. Buchner, J. Kulick, J. L. Schönberger, J. V. de Miranda Cardoso, J. Reimer, J. Harrington, J. L. C. Rodríguez, J. Nunez-Iglesias, J. Kuczynski, K. Tritz, M. Thoma, M. Newville, M. Kümmerer, M. Bolingbroke, M. Tartre, M. Pak, N. J. Smith, N. Nowaczyk, N. Shebanov, O. Pavlyk, P. A. Brodtkorb, P. Lee, R. T. McGibbon, R. Feldbauer, S. Lewis, S. Tygier, S. Sievert, S. Vigna, S. Peterson, S. More, T. Pudlik, T. Oshima, T. J. Pingel, T. P. Robitaille, T. Spura, T. R. Jones, T. Cera, T. Leslie, T. Zito, T. Krauss, U. Upadhyay, Y. O. Halchenko, Y. Vázquez-Baeza, *SciPy 1.0: fundamental algorithms for scientific computing in Python*, 2020.
- [33] B. S. Garbow, K. E. Hillstrom, J. J. More, *Documentation for MINPACK subroutine HYBRD: Double precision version*, 1980.
- [34] M. J. D. Powell, An efficient method for finding the minimum of a function of several variables without calculating derivatives, *The Computer Journal* 7 (1964) 155–162.
- [35] C. K. Law, T. Y. Xiong, C. Wang, Alcohol droplet vaporization in humid air, *International Journal of Heat and Mass Transfer* 30 (1987) 1435–1443.
- [36] C. Chauveau, M. Birouk, I. Gökalp, An analysis of the d2-law departure during droplet evaporation in microgravity, *International Journal of Multiphase Flow* 37 (2011) 252–259.
- [37] F. K. A. Gregson, M. Ordoubadi, R. E. H. Miles, A. E. Haddrell, D. Barona, D. Lewis, T. Church, R. Vehring, J. P. Reid, Studies of competing evaporation rates of multiple volatile components from a single binary-component

- aerosol droplet, *Physical Chemistry Chemical Physics* 21 (2019) 9709–9719.
- [38] A. Bader, P. Keller, C. Hasse, The influence of non-ideal vapor-liquid equilibrium on the evaporation of ethanol/iso-octane droplets, *International Journal of Heat and Mass Transfer* 64 (2013) 547–558.
- [39] L. Ma, X.-q. Qiu, J. Wang, Z.-w. Zheng, Z.-y. Yi, H.-q. Yang, Experimental research on single droplet evaporation factors, *Modern Chemical Industry* 33 (2013) 103–106.
- [40] L. Ma, Y. Chou, X. Cui, Z. Zheng, Research on double-component droplets evaporation properties, *Industrial Heating* 43 (2014) 13–16.
- [41] C. T. Crowe, M. P. Sharma, D. E. Stock, The Particle-Source-In Cell (PSI-CELL) Model for Gas-Droplet Flows, *J. Fluids Eng.* 99 (2010) 325.
- [42] P. Keller, T. Knorsch, M. Wensing, C. Hasse, Experimental and numerical analysis of iso-octane/ethanol sprays under gasoline engine conditions, *International Journal of Heat and Mass Transfer* 84 (2015) 497–510.
- [43] F. L. Sacomano Filho, A. Hosseinzadeh, A. Sadiki, J. Janicka, On the interaction between turbulence and ethanol spray combustion using a dynamic wrinkling model coupled with tabulated chemistry, *Combustion and Flame* 215 (2020) 203–220.
- [44] B. Franzelli, A. Vié, M. Boileau, B. Fiorina, N. Darabiha, Large Eddy Simulation of Swirled Spray Flame Using Detailed and Tabulated Chemical Descriptions, *Flow, Turbulence and Combustion* 98 (2017) 633–661.
- [45] M. Lapuerta, J. P. Hernández, J. R. Agudelo, An equation for the estimation of alcohol-air diffusion coefficients for modelling evaporation losses in fuel systems, *Applied Thermal Engineering* 73 (2014) 539–548.
- [46] E. A. Mason, L. Monchick, Transport properties of polar-gas mixtures, *The Journal of Chemical Physics* 36 (1962) 2746–2757.
- [47] C. C. Wen, C. H. Tu, Vapor-liquid equilibria for binary and ternary mixtures of ethanol, 2-butanone, and 2,2,4-trimethylpentane at 101.3 kPa, *Fluid Phase Equilibria* 258 (2007) 131–139.
- [48] Y. Peng, X. Lu, B. Liu, J. Zhu, Separation of azeotropic mixtures (ethanol and water) enhanced by deep eutectic solvents, *Fluid Phase Equilibria* 448 (2017) 128–134.

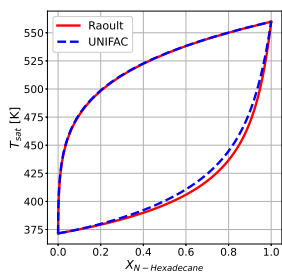


(a) ethanol in air

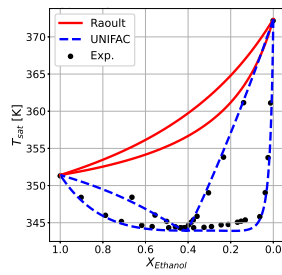


(b) water in air

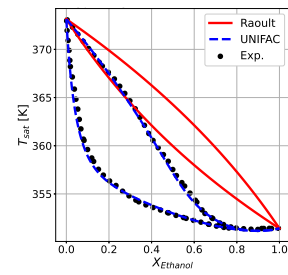
Figure A.2: Values of the diffusion coefficient D for ethanol (a) and water (b) in air computed with different approaches at different temperatures and at atmospheric pressure. Lines refers to computed values, while marks to experimental data. Experimental data for ethanol (a) are extracted from [45] and [46], while for water all data are obtained from [46].



(a) n-hexadecane/n-heptane (NN)



(b) ethanol/iso-octane (PN)



(c) ethanol/water (PP)

Figure A.3: Boiling-point diagrams for three mixtures with different polarity behaviors at 1 atm. The experimental data presented in (b) and (c) are extracted from [47] and [48], respectively.

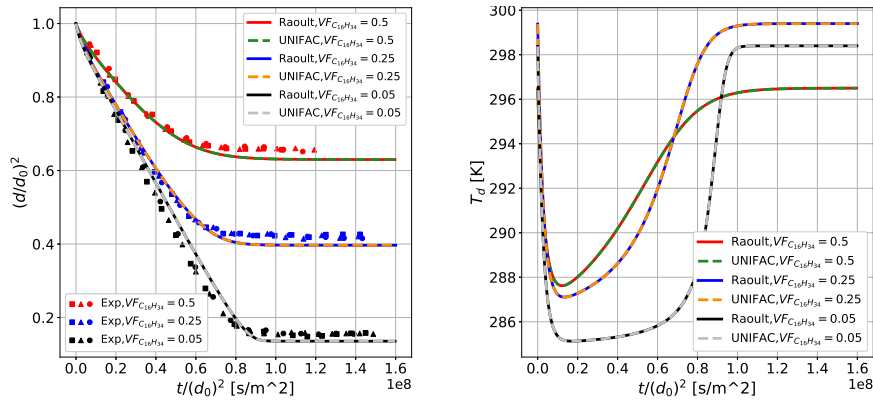


Figure A.4: Comparison of VLE approaches through normalized droplet surface and temperature evolution for a n-hexadecane/n-heptane droplet with initial diameter $d_0 = 50\mu\text{m}$. Temperatures are $T_{d,0} = T_\infty = 296.5\text{K}$ for the initial composition $VF_{C_{16}H_{34}} = 0.5$, $T_{d,0} = T_\infty = 299.4\text{K}$ for the initial composition $VF_{C_{16}H_{34}} = 0.25$ and $T_{d,0} = T_\infty = 298.4\text{K}$ for the initial composition $VF_{C_{16}H_{34}} = 0.05$. Experimental data extracted from [31]

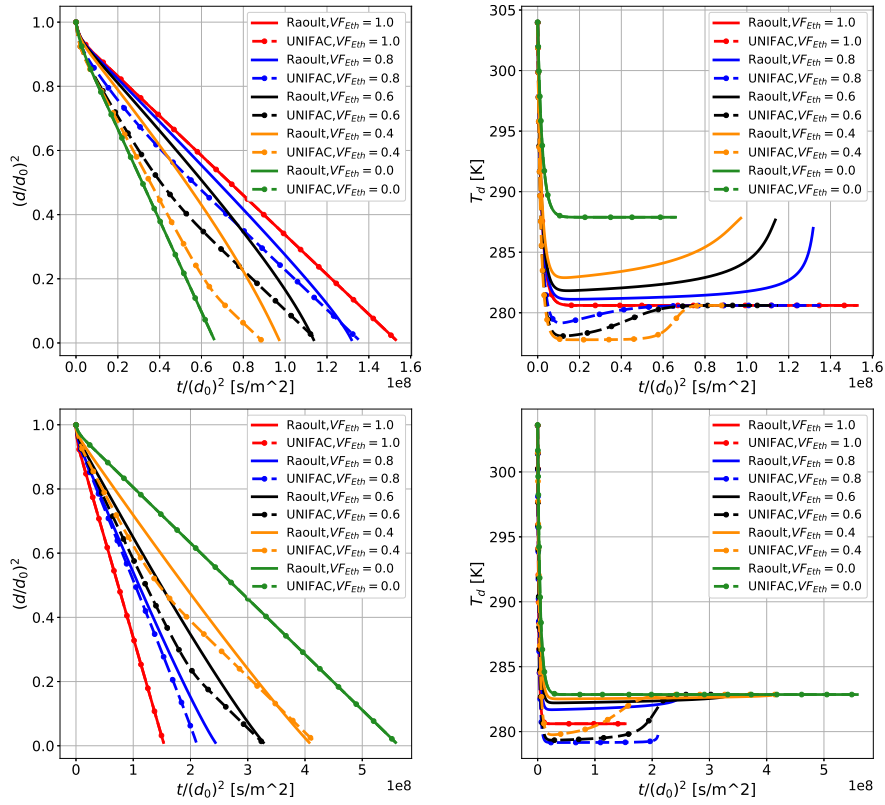


Figure A.5: Comparison of VLE approaches through normalized droplet surface and temperature evolution for a ethanol/iso-octane (top) and ethanol/water (bottom) droplets with initial diameter $d_0 = 50\mu\text{m}$, initial temperature $T_{d,0} = 304\text{K}$, surrounding gas temperature $T_\infty = 304\text{K}$ and varying initial compositions.

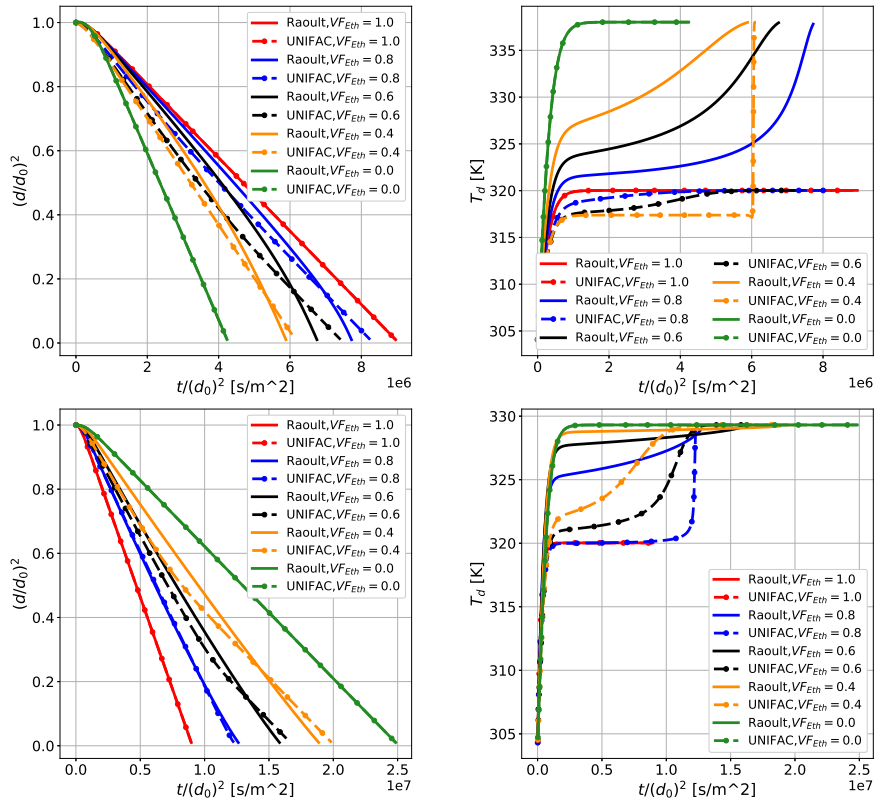


Figure A.6: Comparison of VLE approaches through normalized droplet surface and temperature evolution for a ethanol/iso-octane (top) and ethanol/water (bottom) droplets with initial diameter $d_0 = 50\mu\text{m}$, initial temperature $T_{d,0} = 304\text{K}$, surrounding gas temperature $T_\infty = 703\text{K}$ and varying initial compositions.

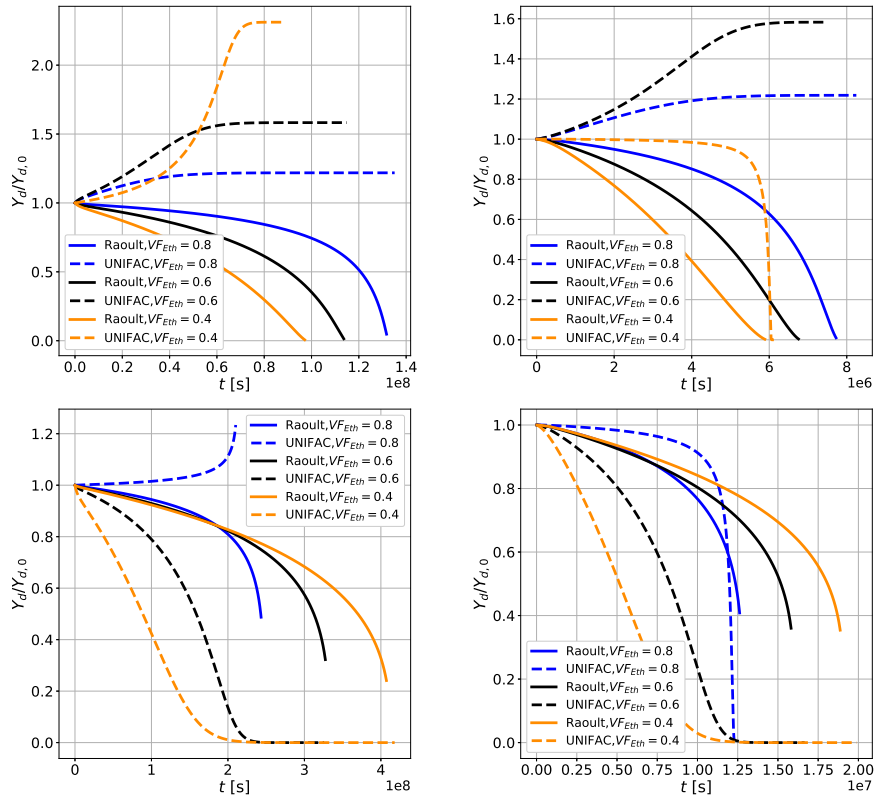


Figure A.7: Comparison of VLE approaches through normalized Ethanol mass fraction inside the droplet for an ethanol/iso-octane (top) and ethanol/water (bottom) droplets with initial diameter $d_0 = 50\mu\text{m}$, initial temperature $T_{d,0} = 304\text{K}$, surrounding gas temperature $T_\infty = 304\text{K}$ (left figures) and $T_\infty = 703\text{K}$ (right figures) and varying initial compositions.

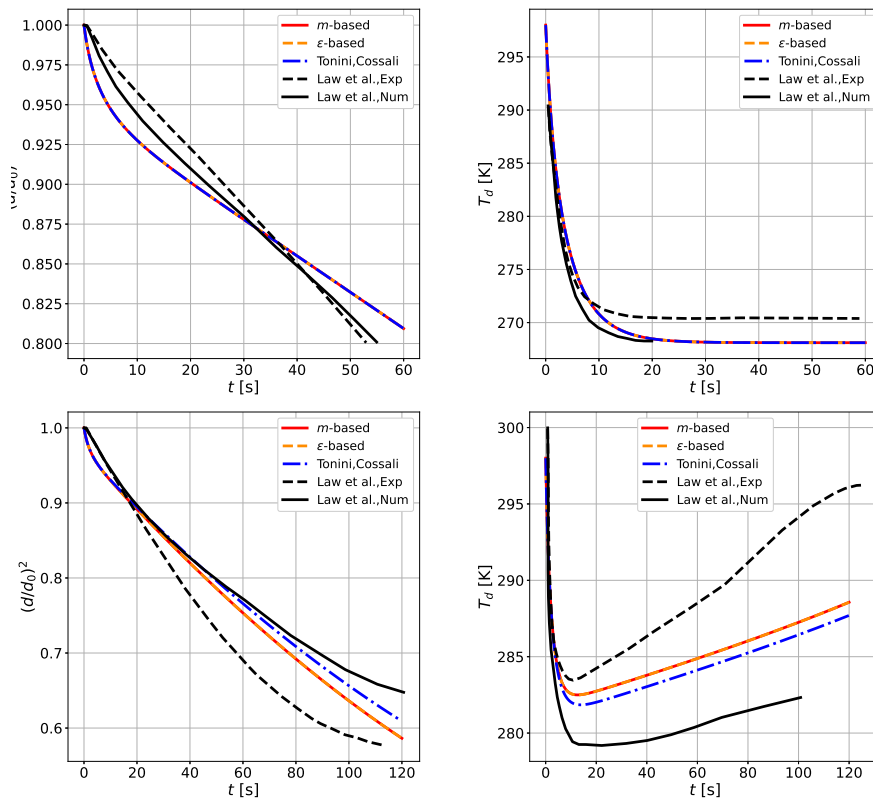


Figure A.8: Comparison of modeling approaches through normalized droplet surface and temperature evolution for a pure Methanol droplet with relative air humidity $\phi = 0.0$ (top) and $\phi = 1.0$ (bottom)

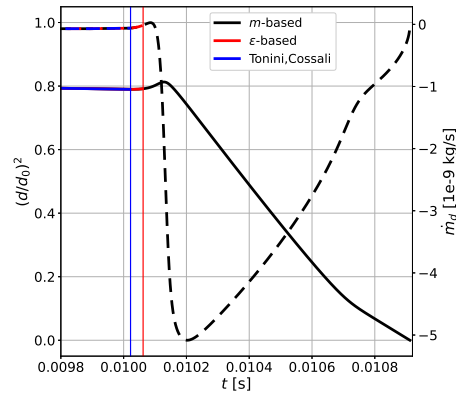


Figure A.9: Normalized droplet surface area (continuous lines) and evaporation rate (dashed lines) for a pure Methanol droplet of initial diameter $d_0 = 20\mu m$ and temperature $T_{d,0} = 300K$ moving through a region of length $L_0 = 0.5cm$ $T_\infty = 300K$ until meeting a flame-front of thickness $L_{flame} = 0.1mm$ wherein both the temperature and the water composition vary following a hyperbolic tangent profile from $T_\infty = 300K$ to approximately $T_\infty = 2000K$ and $Y_{\infty,Wat} = 0$ to approximately $Y_{\infty,Wat} = 0.15$ respectively

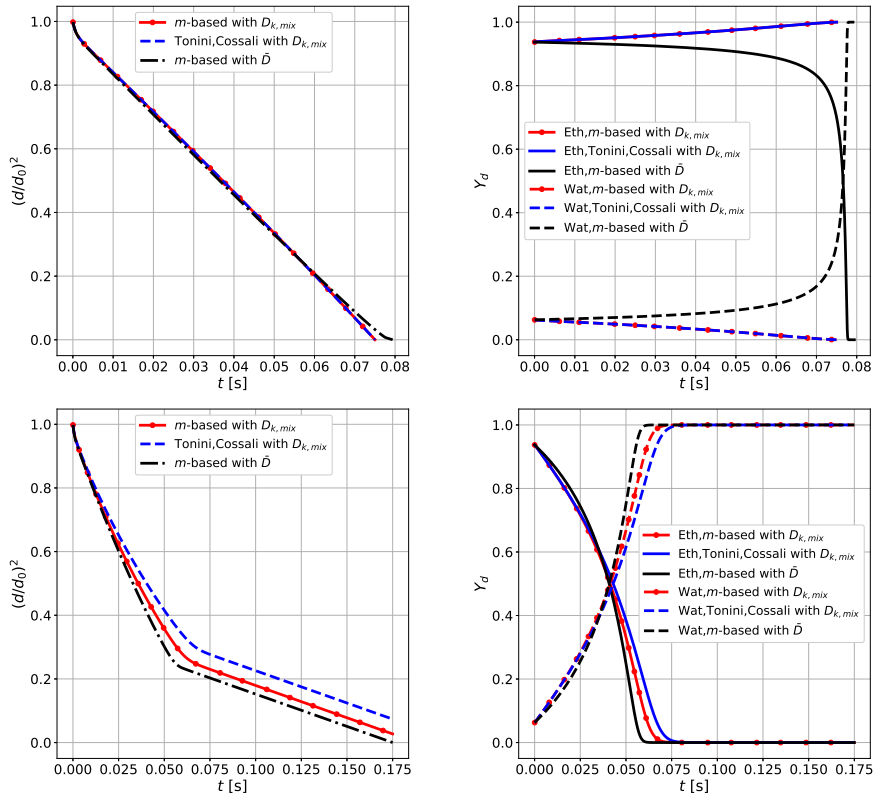


Figure A.10: Normalized droplet surface and internal composition for a $VF = 0.95$ ethanol/water droplet of initial diameter $d_0 = 20\mu\text{m}$ and temperature $T_{d,0} = 300\text{K}$ with surrounding gaseous temperature $T_\infty = 300\text{K}$ and relative humidity of $\phi = 0.0$ (top) and $\phi = 0.4$ (bottom)

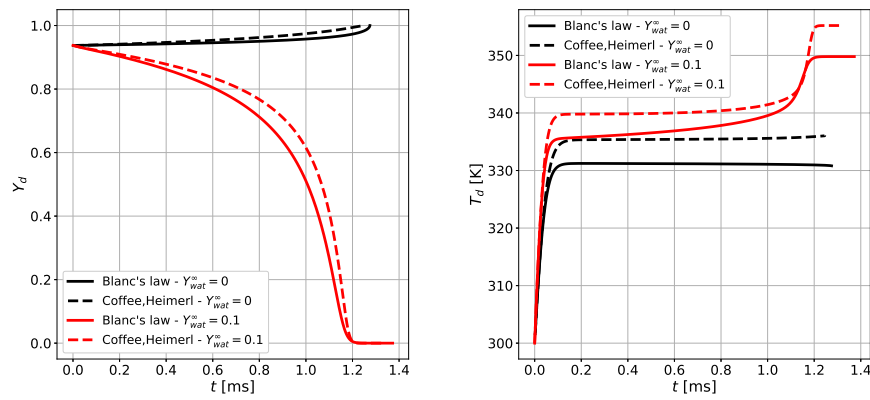


Figure A.11: Ethanol composition inside droplet and droplet temperature for a $VF = 0.95$ ethanol/water droplet of initial diameter $d_0 = 20\mu\text{m}$ and temperature $T_{d,0} = 300\text{K}$ with surrounding gaseous temperature $T_\infty = 1500\text{K}$ and water mass fraction at infinity $Y_{wat}^\infty = 0.0$ and $Y_{wat}^\infty = 0.1$

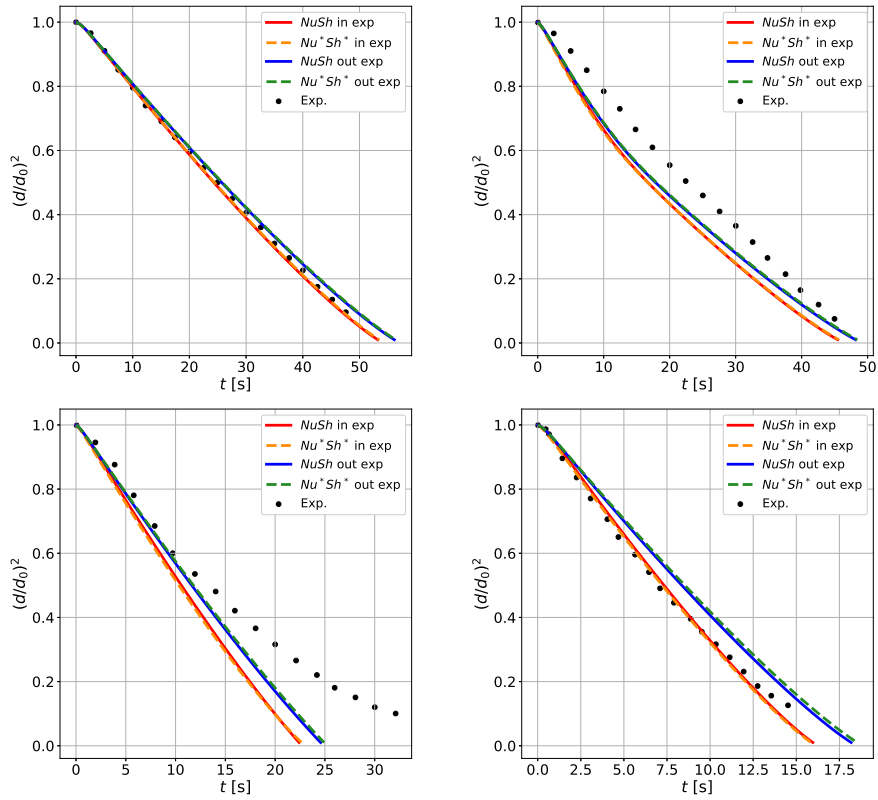


Figure A.12: Normalized droplet surface and temperature for varying initial compositions ($VF_{Eth} = 0, VF_{Eth} = 0.25, VF_{Eth} = 0.75, VF_{Eth} = 1.0$ left-to-right, top-to-bottom) of a ethanol/water droplet of initial diameter $d_0 = 1.2mm$ and temperature $T_{d,0} = 293.15K$ with surrounding gaseous temperature $T_\infty = 400K$

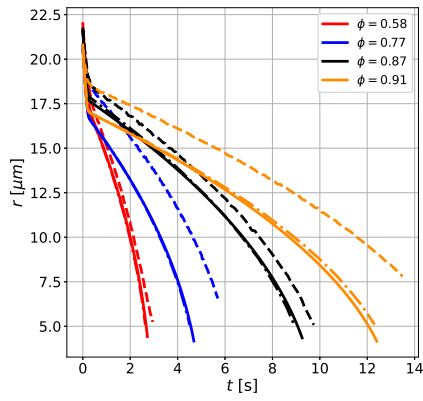


Figure A.13: Droplet instantaneous radius for a 50% ethanol, 50% water (mass fractions) droplet of initial radius $d_0 \approx 22\mu\text{m}$ and temperature $T_{d,0} = 293\text{K}$ with surrounding gas temperature $T_\infty = 293\text{K}$ and various relative humidities representing water vapor at infinity. Depicted are the current model proposition (continuous lines) and the data from Gregson et al. [37] (dashed lines for experimental data, dot-dash lines for numerical results)